Residue-Based Biodiesel: Experimental Investigation into Engine Combustion and Emission Formation

Phuong X. Pham, Ph.D.[1]; and Vu H. Nguyen[2]

Abstract: Utilization of biofuels in autoignition engines is important but it is an exciting challenge to invent technologies that will harness the unique chemico-physical characteristics of these novel fuels. This study aims to investigate combustion phases (e.g., start of combustion and autoignition duration) along with emission characteristics of a residue-based biodiesel in autoignition engines. The fuel has been successfully derived from residue of a cooking-oil production process and two blends (B10 and B20, referring to 10 and 20% in volume of the biodiesel in the biodiesel–diesel mixture, respectively) along with fossil diesel (B0) were tested in a common-rail single-cylinder engine operating under a range of speeds (1,400, 1,800, and 2,400 revolutions per minute), loads (25–100%), and injection timing conditions (16–24° before top dead center). Combustion phases were extensively analyzed employing different approaches including in-cylinder pressure derivatives, heat release rate, and engine vibration signals, while particle and NOx formation, two major issues of autoignition engines, are also investigated. Equivalent timing between local maximum and minimum values of in-cylinder pressure derivative observed for B0, B10, and B20 [1.5° of crank angle (DCA) approximately] may suggest a minimal effect of blending ratio on autoignition duration, albeit the start of combustion occurs earlier for B10 and B20 (1–2 DCA) with respect to B0. Particle concentration of B20 decreases up to 30% compared with that of its fossil counterpart, and this is one of the major benefits of utilizing biodiesel in autoignition engines. **DOI: 10.1061/(ASCE)EY.1943-7897.0000476.**

Author keywords: Biodiesel; Combustion; Ignition delay; Particulate; NOx.

Introduction

With the limitation of fossil-oil reserves and the dramatic increase of energy and feedstock resource demands of the transportation sector, it is crucial to explore nonfossil fuels as well as to improve energy utilization efficiency. It was estimated in 2014 (Wilcox 2014; Reitz 2015) that 60% of 70 million crude-oil barrels were consumed daily by 1 billion vehicles worldwide. Because palm oil is a major feedstock for cooking-oil production in Asia (Timms 2007; Yan and Lin 2009), residues generated from palm-oil replantation and harvesting as well as cooking-oil manufacturing processes could be a potential feedstock for biodiesel production (Sabil et al. 2013). Utilization of biofuels derived from biomass in combustion engines, originally designed for fossil fuels, is useful but it is an exciting challenge for the combustion community to invent novel technologies that will harness the unique chemico-physical characteristics of these novel fuels (Rakopoulos et al. 2014). Recently, residues from a palm-oil production process were successfully converted to biodiesel in Vietnam (Nguyen et al. 2013); the fuel is shown to have comparable properties to those of fossil counterpart, and as such laboratory engine performance tests are required prior to introducing this promising fuel into the market. This residue-based biodiesel has advantages over waste and used cooking oils. Although the waste or used oil can be freely collected from restaurants and houses and then treated to produce low-cost biodiesel (Yaakob et al. 2013), it is usually unstable, contains high free fatty acid and water, and more effort is required to reduce the amount of alcohol, catalyst, reaction time, and particularly reaction temperature in treatment processes (Yaakob et al. 2013; Talebian-Kiakalaieh et al. 2013; Chang et al. 2014). Because the remaining significantly complex combustion phenomenon and challenges to decreasing nitrogen oxide (NOx) and particle emission for compression-ignition (CI) engines is extremely relevant with the advent of biodiesel, this work aims to investigate combustion phases along with NOx and particle formation in CI engines operating with blends of the residue-based biodiesel with fossil diesel.

Combustion in CI engines is a complex, turbulent, three-dimensional, and multiphase process occurring at high temperature and pressure conditions (Heywood 1988; Dec 1997). Dec (1997) presented a conceptual model describing diesel spray combustion in CI engines and this model is applicable for biodiesel combustion (Westbrook 2013). The conceptual model has shown that low-temperature reactions spontaneously ignite portions of premixed fuel–air under quite fuel-rich conditions [local fuel–air equivalent ratio is approximately 2–4 (Dec 1997; Westbrook 2013)], although the overall mixture remains lean due to liquid vaporization and mixing (Ragland and Bryden 2011). The remaining liquid fuel spray is then burning out in the diffusion phase under high-temperature conditions. The heat-release rate during the premixed combustion stage strongly depends on the amount of premixed fuel–air and is a function of the ignition delay (ID) time or the fuel reactivity while the main combustion stage, diffusion combustion (DC), is associated with a lower rate of heat release (Kamimoto and Kobayashi 1991).

Ignition delay, which is defined as the duration between start of injection (SOI) and start of combustion (SOC), is one of the most important parameters in CI engines because accurate measurements of SOI and SOC play a crucial role in examining the engine combustion process. The SOI could be accurately defined using fuel-injection pressure signals (Pham et al. 2014), fuel rate-of-injection

[1]Clean Combustion Research Group—School of Aerospace Mechanical Mechatronic Engineering, Univ. of Sydney, Camperdown, NSW 2006, Australia (corresponding author). E-mail: x.pham@sydney.edu.au

[2]Assistant Professor, Le Quy Don Technical Univ., Hanoi, Vietnam.

Note. This manuscript was submitted on September 16, 2016; approved on March 27, 2017; published online on July 6, 2017. Discussion period open until December 6, 2017; separate discussions must be submitted for individual papers. This paper is part of the ***Journal of Energy Engineering***, © ASCE, ISSN 0733-9402.

trace (Rothamer and Murphy 2013; Macian et al. 2014), or needle lift measurements (Macian et al. 2014). The SOC, however, is much harder to quantify. Because the optical-access-based approach is expensive, the in-cylinder pressure- and vibration-based techniques are the most relevant approaches to estimate SOC. Moreover, an in-cylinder pressure change is often observed before the luminosity detector has noted the flame appearance (Heywood 1988), so the pressure-based technique could be more reliable than the light emission one (Assanis et al. 2003) and is commonly used for combustion analysis through net heat release rate (NHRR) and/or derivatives of the pressure. When using NHRR curves, the occurrence of the autoignition is assumed at the start of rapid heat released (Heywood 1988). The derivatives of cylinder pressure represent sudden changes in the combustion chamber's pressure, which is due to the thermodynamic phenomena within the chamber (Rothamer and Murphy 2013). The first and second derivatives could be utilized for SOC estimations (Assanis et al. 2003); however, the third derivative could also be adopted (Chen et al. 2014). Another technique for detecting SOC is using engine-block vibration signals (Guillemin et al. 2008; Lee et al. 1998; Zhen et al. 2013). Engine combustion is the major source of vibration, albeit multiple excitation sources (piston slap, bearing impact, valve opening and closing, and fuel-injector pulses) could play some roles (Taglialatela-Scafati and Lavorgna 2011).

Although CI engines are more efficient and are an attractive solution to reduce carbon dioxide (CO_2) compared with spark-ignition counterparts (Heywood 1988; Gill et al. 2011), challenges remain in controlling particulate matter (PM) and NOx to a level required by prevailing regulations, which are more and more stringent (Gill et al. 2011). Substantial reductions in PM and NOx emission levels through the Euro 1 (European Council 1991) to Euro 6 (European Council 2007) standards have been required for passenger cars as well as heavy-duty diesel vehicles (Rodriguez-Fernandez et al. 2010). For heavy-duty vehicles, PM and NOx have been reduced 35 and 20 times, respectively, from Euro 1 to Euro 6 emission standards. The standard for NOx is five times lower for Euro 6 compared with Euro 4, and this is twice that for PM.

The NOx formation mechanism is quite mature for diesel fuel; however, that for biodiesel is not fully understood and reports for the trend in NOx concentration are contradictory in the literature (Lapuerta et al. 2008) with a widespread agreement that no single factor affects biodiesel NOx formation. An increase in NOx concentration has been observed by Miyamoto et al. (1998), while Schonborn et al. (2009) show a reduction in NOx when increasing the fuel oxygen content under constant injection and ignition timing conditions. Giakoumis et al. (2014) examined NOx formation in an engine operating with biodiesel blends under transient conditions and observed an increasing trend in NOx concentration when increasing the biodiesel blending ratio. This trend was also observed by Kousoulidou et al. (2014) for hydrotreated vegetable oil tested in a modern diesel engine operating under the New European Driving Cycle (Barlow et al. 2009). A study on low blending ratio (5–10%) of two biodiesel types with different saturated levels in diesel tested over the Federal Test Procedure (FTP), the Urban Dynamometer Driving Schedule (UDDS), and the Supplemental Emission Test (SET) cycles (Karavalakis et al. 2016) has shown a significant effect of saturated level on NOx emitted; both increasing and decreasing trends were observed depending on fuel types and also testing cycles used. In modern diesel engines, Hoekman and Robbins (2012) stated that several factors related to fuel compositions and engine control strategies are important to the NOx mechanism, though no single theory provides an adequate explanation of the biodiesel NOx effect under all conditions. There is evidence to suggest that effects on physical properties (bulk modulus, viscosity, surface tension, heating value, thermal conductivity, and density), chemical parameters (cetane number, fuel bound oxygen, degree of saturation), injection timing, ignition delay, adiabatic flame temperature, radiative heat loss, and other combustion phenomena all play some role.

It is commonly agreed in the literature that adding biodiesel into fossil diesel leads to significant decreases in particles emission; however, soot processes are still not fully understood (Westbrook 2013; Pham et al. 2013; Nguyen and Pham 2015). Those processes could be described through the following steps (Tree and Svensson 2007): fuel pyrolysis, nucleation, coalescence, surface growth, agglomeration, and oxidation. The oxygen atoms in biodiesel could cause suppression of soot formation by effectively removing carbon from reaction pathways that lead to soot precursors (Zhu et al. 2010). The presence of surface oxygen on soot leads to surface burning that occurs progressively from the outermost periphery, which may cause soot diameter reduction, and therefore mass reduction for biodiesel with respect to fossil diesel (Krahl et al. 2001; Maricq 2011). Fuel oxygen content can have an indirect effect on soot formation through the changes it creates during the combustion process (Tree and Svensson 2007; Donahue and Foster 2000; Omidvarborna et al. 2016). It was found by Donahue and Foster (2000) that higher oxygen contained in a fuel decreased pyrolysis and the combustion duration while it increased oxidation. Recent scientific articles (Chang et al. 2014; Agarwal et al. 2014; Chattopadhyay and Sen 2013; Tziourtzioumis and Stamatelos 2014; Lee et al. 2014) have shown that biodiesel blends have significant effects on particle concentrations. Agarwal et al. (2014) tested Karanja biodiesel blends along with fossil diesel in a common-rail direct-injection engine and showed that the particle number concentration reduces significantly when using the B10 blend with respect to fossil diesel. An addition of even a very small fraction of the Karanja fuel leads to a substantial reduction in particulate emissions. The effects of blending of 20% of biodiesel and diesel on the operation, diesel filter loading, and fuel additive–assisted regeneration behavior of a single-cylinder CI engine have been conducted by Tziourtzioumis and Stamatelos (2014) and the study showed a decrease of 20°C in soot oxidation temperature for the B20 blend, which suggests a higher reactivity of biodiesel soot.

Because studies on combustion phases are still limited (e.g., report on autoignition duration for biodiesel blends in CI engine is scarce in the literature, according to the authors' knowledge), this work will extensively investigate combustion phases (e.g., start of combustion and autoignition duration) using different approaches (in-cylinder pressure derivatives, heat release rate, and vibration signal) along with an analysis of NOx and particle formation in a common-rail single-cylinder engine. This may shed more light on combustion phases and particle and NOx formation in CI engines when operating with the residue-based biodiesel.

Fuel Properties and Experiment Setup

As briefly mentioned previously, the biodiesel used in this study was derived from residues of a palm cooking-oil production process. The residues were found to still be rich in fatty acid esters, and biodiesel used in this work was successfully derived from the residues using triple cycles of heterogeneous-catalyzed transesterification. The fuel-conversion process was aided by a high-hardness solid ceramic metal catalyst, which was invented by Yoo et al. ["Ceramic catalyst used in manufacture of fatty acid alkyl esters and method for preparing high purity fatty acid alkyl esters using the same," U.S. Patent No. 2,012,013,010,1A1 (2012)] using a sintering process. The initial cost of the heterogeneous-catalyzed

Table 1. Selected Properties for Fuel Blends: D (Pure Diesel), B10, B20, and B100 (Pure Biodiesel)

Property	Unit	Testing method	B100	B20	B10	D(B0)
Ester content	% by weight	EN 14103 (European Standard 2011)	98.91	—	—	—
Glycerin content	% by weight	ASTM D6584 (ASTM 2013)	0.0	—	—	—
Phosphorus content	% by weight	ASTM D4951 (ASTM 2009)	0.0002	—	—	—
Sodium/potassium, combined	mg/kg	EN 14538 (European Standard 2006)	0.1	—	—	—
Oxidation stability, 0 months	h	EN 14112 (European Standard 2003b)	6.02	24.07	111.9	—
Oxidation stability, 8 months	h	EN 14112 (European Standard 2003b)	—	6.8	87	—
Palmitic, C16:0	% by weight	—	28.09	—	—	—
Stearic, C18:0	% by weight	—	9.53	—	—	—
Oleic, C18:1	% by weight	—	43.47	—	—	—
Linoleic, C18:2	% by weight	—	18.02	—	—	—
Iodine value	gI/100 g	EN 14111 (European Standard 2003a)	48.0	—	—	—
Saponification number	mgKOH/g	ASTM D664-04 (ASTM 2004)	177.3	—	—	—
Acid number	mgKOH/g	ASTM D664 (ASTM 2004)	0.06	—	—	—
Water content	% by weight	ASTM D95-05 (ASTM 2005c)	0.20	—	—	—
Flash point	°C	ASTM D93 (ASTM 2003)	152	—	—	—
Kinematic viscosity at 40°C	mm^2/s	ASTM D445 (ASTM 2006)	4.1	3.38	3.25	3.14
Relative density at 15°C	—	ASTM D1298 (ASTM 1999)	0.869	0.845	0.841	0.836
Higher heating values	MJ/kg	—	—	43.11	43.86	45.19
Cloud point	°C	ASTM D2500 (ASTM 2005b)	18	—	—	—
Pour point	°C	ASTM D97 (ASTM 1995)	—	−3	−3	—
Cetane number	—	ASTM D613 (ASTM 2005a)	66.9	54.5	53.7	52.4

approach could be higher compared with that of conventional transesterification; its catalysts, however, can be recycled many times and it is a favorite conversion technique due to its simpler separation and continuous operation as well as requirement for less washing. A comprehensive analysis for production techniques is beyond the scope of this work, but Knothe and Razon (2017) recently performed a review on progress of biodiesel fuels. Important physicochemical properties of the B0, B10, and B20 blends along with the pure biodiesel (B100) have been tested carefully using relevant testing methods, as shown in Table 1. An ester concentration of 98.91% was observed for the pure residue-based biodiesel and most fuel properties meet the ASTM D6751 standard (ASTM 2007), except oxidative stability (OS) and cloud point. As such, additives including anticorrosive ethylenediamine, cold flow poly-alpha olefins, and antioxidant tert-butylhydroquinone were used to increase oxidative stability and lower cloud point. Oxidative stability values shown in Table 1 for B0, B10, and B20 were measured 0 and 8 months after production. It is clear from Table 1 that B10 well meets the ASTM D6751 (ASTM 2007) standard for both 0 and 8 storage months (e.g., B10 has an OS of 111.9 h, while ASTM D6751 requires an OS value of 6 h). Blend B20, however, has an OS of only 24.07 and 6.8 h at 0 and 8 months, respectively.

The experiment was conducted using an AVL 5402 common-rail single-cylinder research engine (AVL, Austria) schematically

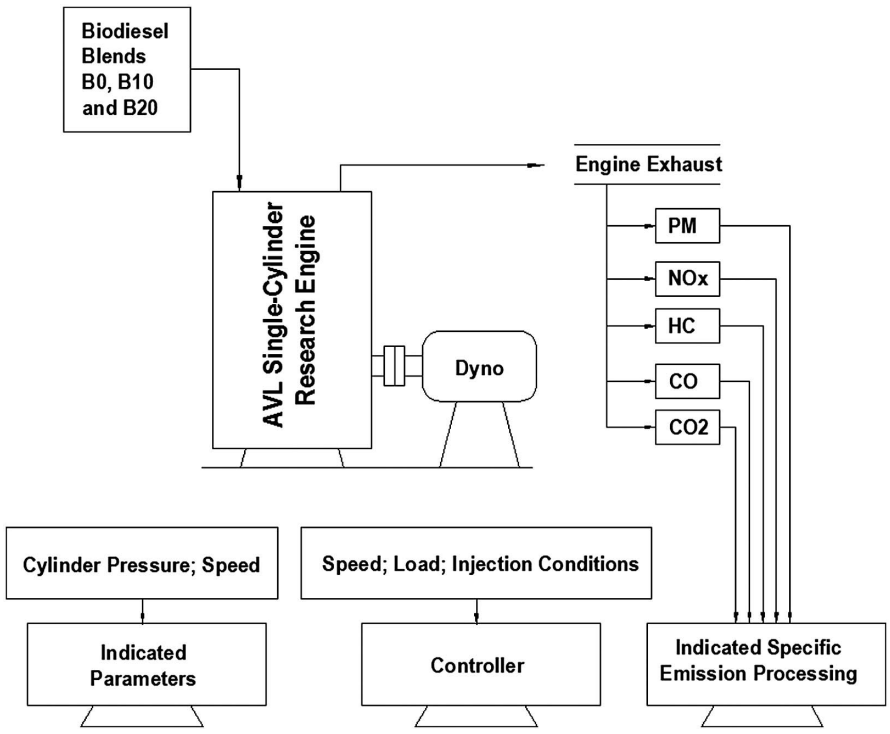

Fig. 1. Schematic of experimental engine

Table 2. Single-Cylinder Research Engine Specifications for AVL 5402

Specification	Value
Number of cylinders	1
Valves	4 dual overhead camshaft
Fuel-injector type	Bosch high-pressure common rail
Nozzle type	Valve-covered orifice
Maximum rail pressure	135 MPa
Number of holes/diameter	5/0.17 mm
Spray included angle	142°
Bore × stroke	85 × 90 mm
Connection rod	138 mm
Swept volume	0.51 L
Swirl ratio	1.78
Rated power	9 kW (at 3,200 rpm)
Compression ratio	17.3:1
Dynamometer type	APA100 (AVL, Austria)

shown in Fig. 1; the engine specifications are described in Table 2. This is a high-speed CI engine having a central fuel injector and four valves equipped with a dual-overhead camshaft valve train. In this study, the engine was operated under a wide range of speeds [1,400–2,400 revolutions per minute (rpm)] and the injection timing was varied from 16 to 24° of crank angle (DCA) before top dead center (BTDC), while injection duration was kept constant at 800 μs and the injection pressure was remained constant at 40 MPa (400 bars). Engine speed and crank rotation angle are controlled using a 0.5 DCA resolution encoder. Fuel consumption was measured using an AVL Fuel Balance 733S. Under the injection conditions mentioned previously, the amount of fuel injected is fixed constant at 4.66 mL/cycle among the blends and engine speed conditions. In-cylinder pressures were measured using a flush-mounted water-cooled AVL QC34C quartz piezoelectric pressure transducer. Nitrogen oxide was detected using a chemiluminescence analyzer, while particle concentration was detected employing an AVL 439 Opacimeter.

Engine Combustion Analysis

Combustion Phases in a CI Engine

Figs. 2(a–c) show typical timing and stages between SOI and end of combustion in one cycle of the common-rail engine used in this study. The data shown here are for the fossil diesel under 1,800 rpm engine speed and 20 DCA BTDC of SOI. The in-cylinder pressure signal is also shown in Figs. 2(a–c). The NHRR, second derivative of cylinder pressure, and vibration signal are shown in Figs. 2(a–c), respectively.

Fig. 2(a) shows distinguishable combustion phases in the one engine cycle. An amount of fuel mixed with air during the ignition delay period, from SOI to SOC, leads to a fast burning or premixed combustion process resulting in a rapid heat release shown at approximately 9 DCA BTDC, representing the SOC, and a peak at NHRR observed at approximately 5 DCA BTCD.

Cylinder pressure and its second derivative are shown in Fig. 2(b). It is evident from Fig. 2(b) that the peak of the derivative curve coincides with the sudden change in the cylinder pressure, which is due to autoignition, and this is in a good agreement with observations in Syrimis et al. (2006) and Ando et al. (1989). It was found previously that the local peak of second derivative of cylinder pressure always occurred at or slightly after the autoignition event

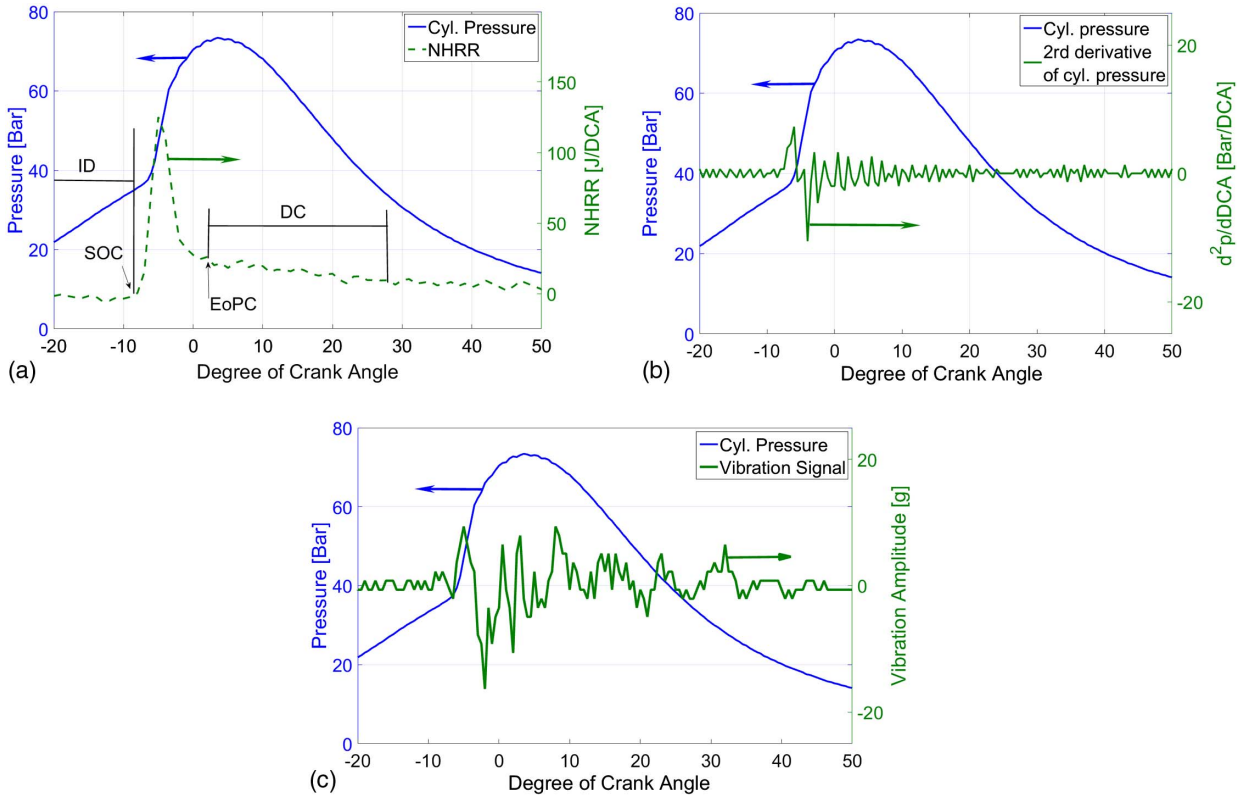

Fig. 2. Identification of SOC, ID, autoignition duration, end of premixed combustion (EoPC), and DC using (a) in-cylinder pressure and net heat release rate; (b) in-cylinder pressure and its second derivative; (c) in-cylinder pressure and engine vibration signal (results shown for B0, 1,800 rpm engine speed, and an injection timing of 20 DCA BTDC)

J. Energy Eng., 2017, 143(5): 04017047

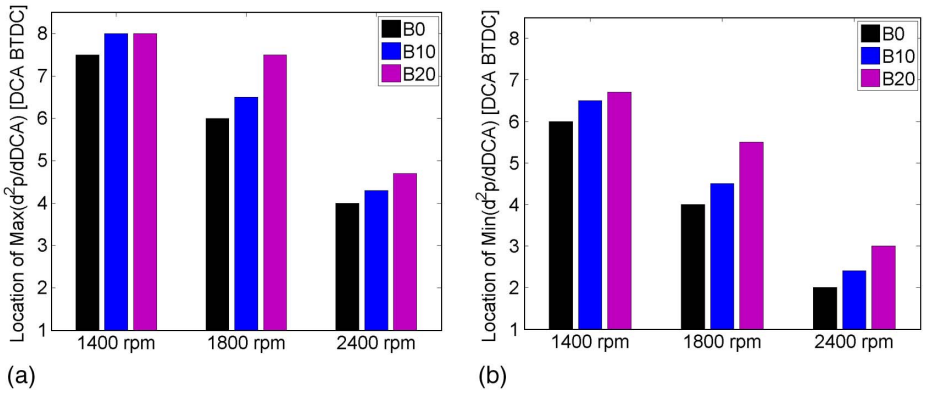

Fig. 3. Locations of (a) maximum; (b) minimum values of the second derivative of in-cylinder pressure (injection timing = 20 DCA BTDC)

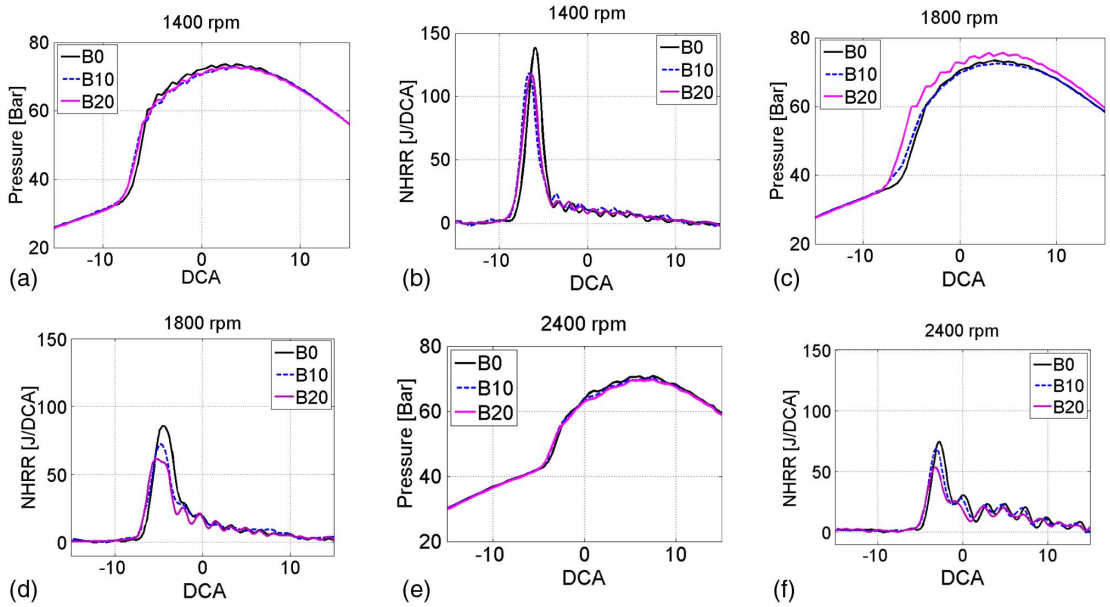

Fig. 4. In-cylinder pressure and NHRR of biodiesel blends (B0, B10, and B20) at three engine speed conditions: (a and b) 1,400 rpm; (c and d) 1,800 rpm; (e and f) 2,400 rpm

(Syrimis et al. 2006; Ando et al. 1989). The maximum value of the derivative could represent the start of autoignition, while the minimum one could correspond to the end of autoignition (Ando et al. 1989). Both local maximum and minimum values of the second derivative are clearly observed in Fig. 2(b) and these could be good indicators for start and end of autoignition.

Vibration signal is shown in Fig. 2(c) along with in-cylinder pressure. It is quite clear that the first rapid rise of the signal is close to that of the NHRR [Fig. 2(a)] as well as the second derivative of cylinder pressure [Fig. 2(b)]. The vibration signal is quite similar to the second derivative in their locations for the maximum and minimum values during the autoignition process, and thus can give supplementary information to characterize autoignition.

Combustion of Biodiesel Blends

Fig. 3(a) shows the crankshaft locations in DCA BTDC, where maximum values of the second derivative of in-cylinder pressure are observed, similar but for minimum values that are shown in Fig. 3(b). As discussed in the previous section, the maximum and minimum values could indicate the start and the end of autoignition, respectively. The data shown in Figs. 3(a and b) are for different biodiesel blends (B0, B10, and B20) under various engine speed conditions (1,400, 1,800, and 2,400 rpm). It is evident from Fig. 3(a) that increasing the biodiesel blending ratio results in an earlier occurrence of maximum values of the second derivative of in-cylinder pressure. Because the injection timing is observed to be independent of the fuel types in this study, the earlier occurrence of the maximum values with higher biodiesel blending ratios suggests a shorter ignition delay for the biodiesel blends and this is attributable to higher reactivity of the biodiesel compared with that of fossil diesel. Figs. 3(a and b) also show that the duration between occurrences of maximum and minimum values is independent of fuel blends and engine operating conditions. Although the appearance of maximum as well as minimum values is different among the fuel blends tested and engine speeds used as shown in Figs. 3(a and b), the duration is approximately 1.5 DCA for all fuel blends and all engine speed conditions. The information for autoignition duration of biodiesel blends is scarce in the literature to the authors' knowledge.

Figs. 4(a, c, and d) show the $p - \theta$ data for biodiesel blends B0, B10, and B20 under three engine speed conditions of 1,400, 1,800,

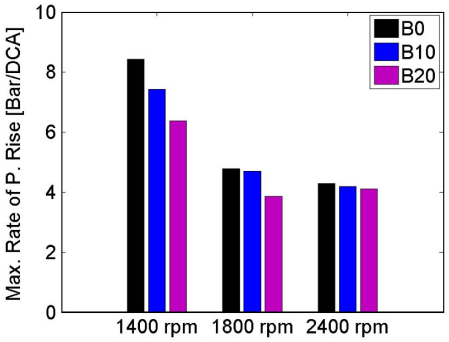

Fig. 5. Maximum rate of pressure rise of biodiesel blends (B0, B10, and B20) at 1,400, 1,800, and 2,400 rpm of engine speed

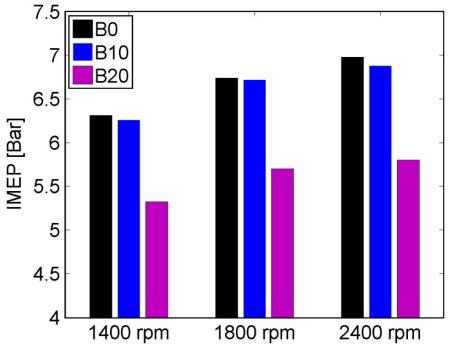

Fig. 6. Indicated mean of effective pressure of biodiesel blends (B0, B10, and B20) at 1,400, 1,800, and 2,400 rpm engine speed

and 2,400 rpm, respectively. Figs. 4(b, d, and f) are similar but for NHRRs. In agreement with observations from Fig. 3(a) for maximum values of the second derivative of in-cylinder pressure, Figs. 4(a–f) show that the start of autoignition of blends B10 and B20 occurs earlier compared with that of fossil diesel (B0). It can also be seen that both premixed combustion and diffusion combustion are visible in Figs. 4(b, d, and f). For example, the premixed combustion duration of blends B10 and B20 is approximately 5 DCA and a pretty high heat release rate is generated during this process with a peak at approximately 5 DCA BTDC. The diffusion combustion follows without an observable peak and shows a much lower heat release rate compare with that of premixed combustion.

The maximum rate of in-cylinder pressure rise is an important parameter that reflects the fuel burning rate. The maximum value is often observed during the premixed combustion process, which is also known as fast burning duration in CI engines (Heywood 1988; Rothamer and Murphy 2013). Results for the mean peak rate of pressure rise are presented in Fig. 5 for the biodiesel blends (B0, B10, and B20) at 1,400, 1,800, and 2,400 rpm engine speed conditions. It is clear in this figure that increasing the biodiesel–diesel blending ratio leads to a decrease in the maximum rate of in-cylinder pressure rise. B0 shows the highest mean of maximum rate of in-cylinder pressure rise, followed by B10, then B20's rate is the lowest. The highest mean of maximum rate of B0 is attributable to its lowest cetane number (longest ID) and therefore the highest proportion of premixed combustion among the fuel blends tested here. With a longer ignition delay time, fuel and air have more time to premix prior to autoignition, resulting in a higher rate of pressure

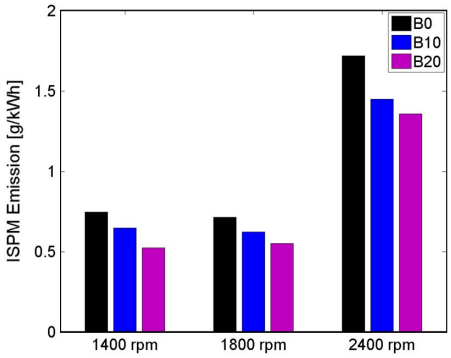

Fig. 7. Indicated specific particle mass concentrations of B0, B10, and B20

rise as well as a higher heat release rate, which is shown quite clearly in Fig. 4 for HRR and Fig. 5 for rate of pressure rise of the biodiesel blends tested in this study.

The indicated mean of effective pressure (IMEP) measured at 1,400, 1,800, and 2,400 rpm engine speed is plotted in Fig. 6 for three blends, B0, B10, and B20, respectively. It is clear that increasing blending ratio leads to a reduction in IMEP; B10, however, shows only small decreases (1.5% maximum at 2,400 rpm) in its IMEP when compared with that of B0. The small decrease in IMEP of B10 with respect to B0 could be attributed to an improvement in lubricant quality when utilizing a low biodiesel blending ratio. Increases in engine power and thermal efficiency have also been observed when utilizing low biodiesel blending ratios such as B2–B5 (Knothe et al. 2010). At a high biodiesel fraction such as B20 in this study, however, the benefit gained from improving lubricant quality is minimal with respect to the penalty in engine power, which is attributed to heating value reduction.

Engine Emission Analysis

Particulate Emission Formation

Fig. 7 shows concentrations of indicated specific particle mass (ISPM) emitted from the single-cylinder CI engine operating with biodiesel blends B0, B10, and B20 under three engine speed conditions, 1,400, 1,800, and 2,400 rpm, respectively. It is clear for all three operating conditions that the ISPM level reduces significantly with increasing the blending ratio of the biodiesel–diesel mixture. Using biodiesel blend B20, for example, decreases ISPM concentration by approximately 30% compared with neat diesel (B0). Additional oxygen atoms provided by the biodiesel may improve autoignition quality and combustion efficiency as well as soot oxidation, and this could be attributable for the reduction of particle concentrations shown in Fig. 7 as discussed.

NOx Formation

Fig. 8 shows indicated specific NOx (ISNOx) concentrations emitted from the engine when operating with biodiesel blends B0, B10, and B20 under three engine speed conditions (1,400, 1,800, and 2,400 rpm, respectively). It is clear from Fig. 8 that B10 produced a slightly lower amount of ISNOx, while using B20 leads to a higher amount of ISNOx compared with B0. These results are in good agreement with the previous finding reported by Roy et al. (2013). They found that the B5 blend of canola-based biodiesel shows lower concentrations of NO, NO_2, and total NOx compared

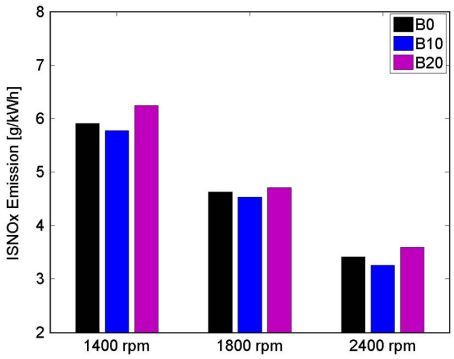

Fig. 8. Indicated specific NOx concentrations of B0, B10, and B20

with those of fossil diesel. However, their biodiesel blend B20 has 12–26% NOx increase depending on engine speed conditions. The small reduction in IMEP for B10, which is attributable to lubricant enhancement as discussed previously, might lead to the decrease in specific NOx concentration (g/kWh) observed for B10 as shown in Fig. 8, although the detailed mechanism behind this reduction is not quite clear.

Blend B0 shows a higher rate of pressure rise and generates a higher heat during heat release (Fig. 4) compared with B20, but B0 shows its lower NOx concentration, as mentioned. Normally, NOx has an inverse correlation with flame temperature (Jozsa and Kun-Balog 2015). However, there exist other factors involving the NOx mechanism such as physical properties (bulk modulus of fuel compressibility, viscosity, and surface tension) and chemical properties (cetane number) of the fuel as well as engine operating conditions, and this is beyond the scope of this work. Further information on the influences of biodiesel physical and chemical properties on NOx formation can be found in Garner et al. (2009), Varatharajan and Cheralathan (2012), Tat et al. (2000), and Kegl (2006).

Effects of Injection Timing on Particle and Nitrogen Oxides Formation

This section will report the effect of fuel injection timing on engine combustion and emission formation and this will focus on the B20 blend. Figs. 9(a and b) plot cylinder pressure and heat release rate, respectively, versus DCA for B20 at 1,800 rpm engine speed and a range of injection timing from 16 to 24 DCA BTDC. It is evident from Figs. 9(a and b) that an advanced injection timing leads to an earlier autoignition and a higher peak cylinder pressure [Fig. 9(a)] and maximum heat release rate during the premixed combustion [Fig. 9(b)]. It can also be seen from Fig. 9(b) that Fig. 9(a)'s variation in fuel injection timing affects ignition delay times. An estimation for ignition delay time was performed using NHRR as shown in Fig. 9(b) and a difference of approximately 4 DCA in ignition delay times was observed when the injection timing advances by 8 DCA, from 16 to 24 DCA BTDC. This is understandable because when the fuel is injected closer to top dead center, the cylinder temperature is higher, which results in a shorter ignition delay. A shorter ignition delay leads to a smaller premixed combustion proportion, which is evident from Fig. 9(b).

To examine the effect of injection timing on emission levels, ISNOx concentrations are plotted versus injection timing in Fig. 10(a) and versus ignition delay in Fig. 10(b). Linear correlations are observed for ISNOx concentrations when plotted versus injection timing in Fig. 10(a) and ignition delay in Fig. 10(b). An advance in injection timing leads to a longer ignition delay and a significant increase in ISNOx. When injection timing advances from 16 to 24 DCA BTDC, for example, the ignition delay time increases from 11 to 14 DCA and the ISNOx level is more than double from 4 to 8.5 g/kW h. The correlation between ID and NOx is notable in this study, albeit this is not the sole factor affecting the NOx mechanism, as discussed previously. During the ID time or preparation period, the liquid undergoes complex physical and chemical processes such as atomization (Kourmatzis et al. 2013, 2015; Pham 2015), evaporation, mixing, and preliminary chemical reactions. Ignition occurs after the preparation period and leads to fast exothermic reactions. The increase in ISNOx with increasing ID could be attributed to thermal NOx formation. A longer ignition delay leads to a larger premixed combustion proportion. The heat release rate during the premixed combustion will preheat the mixture in diffusion combustion and this in turn increases the cylinder pressure and temperature. Cylinder temperature is not estimated in this work; however, it is evident from Figs. 9(a and b) that a shorter ignition delay leads to a higher heat release rate [Fig. 9(b)] and higher maximum pressure [Fig. 9(a)]. This finding is in agreement with earlier work done by Halstead et al. (1975), Hoskin et al. (1992), and Kong and Reitz (1993).

Indicated specific particle mass concentrations are plotted versus injection timing in Fig. 11(a) and versus ignition delay in Fig. 11(b). A minimum ISPM concentration is observed at approximately 20 DCA BTDC of injection timing [Fig. 11(a)], which corresponds to an ID duration of 12 DCA [Fig. 11(b)]. When ignition delay increases, the fuel and air have a longer time to mix prior to autoignition and this results in a higher premixed combustion proportion or higher cylinder temperature, which leads to faster chemical kinetics. In general, faster kinetics can help to achieve a higher combustion efficiency and lower particle emission. When the ignition delay exceeds a certain value, however, the fast burning rate during the premixed combustion leads to a higher engine

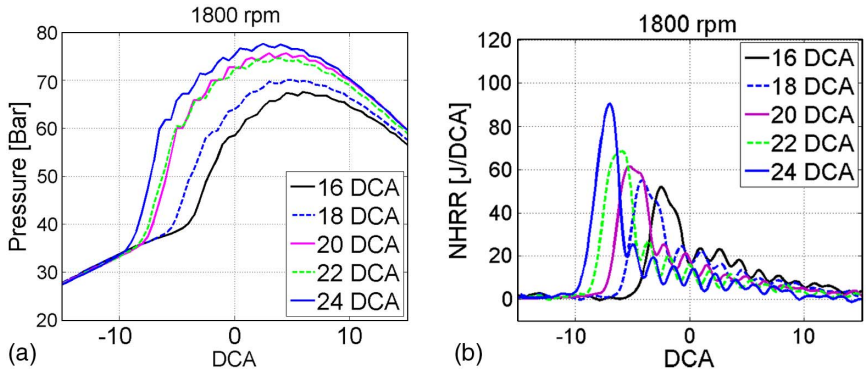

Fig. 9. (a) In-cylinder pressure and (b) net heat release rate of B20 at 1,800 rpm and different injection timing

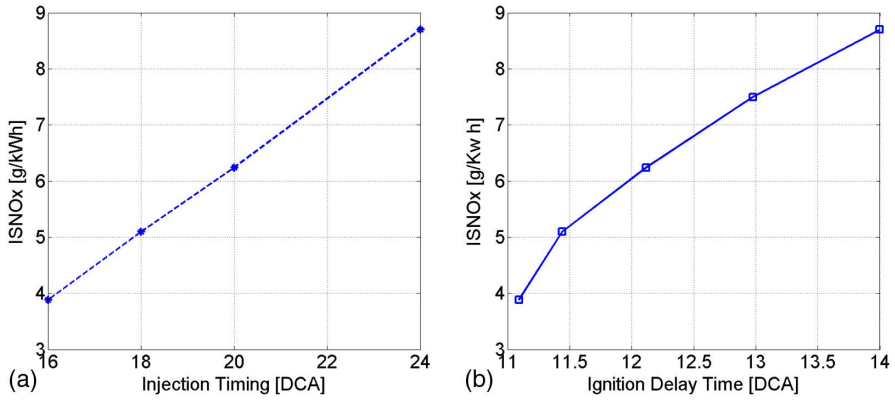

Fig. 10. Indicated specific NOx concentrations of B20 at 1,800 rpm engine speed versus (a) injection timing and (b) ignition delay

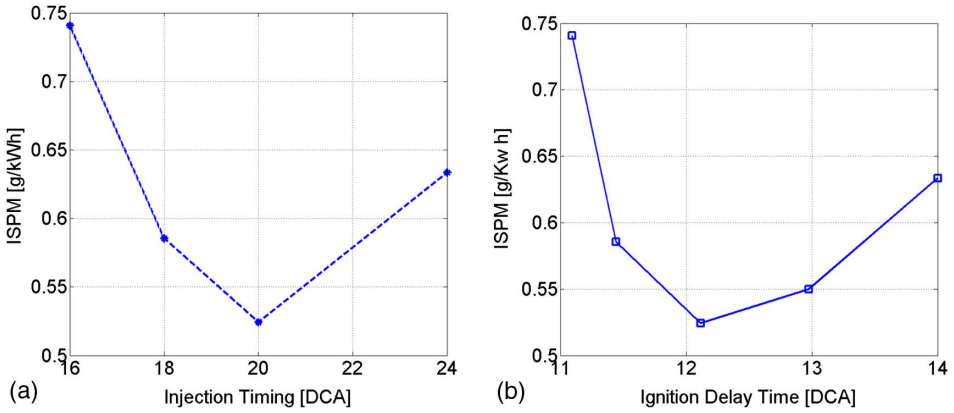

Fig. 11. Indicated specific emission concentrations of B20 at 1,800 rpm engine speed versus (a) injection timing and (b) ignition delay

combustion variability (Pham et al. 2014) and this could be an explanation for an increase in particle concentration shown in Fig. 11(b) when injection timing exceeds 20 DCA BTDC.

Conclusion

Blends (B0, B10, and B20) of a biodiesel, which was manufactured from residues of a cooking-oil production process, and fossil diesel have been examined experimentally using a common-rail autoignition engine. This is a single-cylinder fuel research engine that was operated under a broad range of engine speeds (1,400, 1,800, and 2,400 rpm) and fuel-injection timing conditions (16–24 DCA BTDC). Combustion phases of air-fuel cycles, NOx, and particle concentrations from the engine were reported. Combustion phases are consistently observed when using three different approaches including in-cylinder pressure derivatives, net heat release rate, and engine vibration signals, and this shows the feasibility of those approaches for measuring start and end of autoignition, ignition delay, or premixed combustion proportion. Increasing the biodiesel–diesel blending ratio delays the start of combustion and reduces the heat release rate and maximum rate of pressure rise. At 1,400 rpm, B20 shows its 2-DCA earlier SOC and approximately 0.2 MPa (2 bars) per DCA higher maximum rate of pressure rise compared with those of D. Similar duration between occurrences of local maximum and minimum values of in-cylinder pressure derivatives suggests a minimal effect of biodiesel blending ratio on autoignition duration. An autoignition duration of approximately 1.5 DCA was observed in this study and this is the first report for biodiesel autoignition duration in CI engines to the best of the authors' knowledge. Biodiesel blends also showed their benefit of significantly decreasing engine exhaust particle emission.

Acknowledgments

This work is financially supported by the Directorate of Programs on "Biofuels development until 2015 and vision for 2025," the Ministry of Industry and Trade—Vietnam (under project number DT.08.14/NLSH).

References

Agarwal, A. K., Dhar, A., Gupta, J. G., Kim, W., Lee, C., and Park, S. (2014). "Effect of fuel injection pressure and injection timing on spray characteristics and particulate size? Number distribution in a biodiesel fuelled common rail direct injection diesel engine." *Appl. Energy*, 130(11), 212–221.

Ando, H., Takemura, J., and Koujina, E. (1989). "A knock anticipating strategy based on the real-time combustion mode analysis." *SAE Paper 890882*, Society of Automotive Engineers, Warrendale, PA.

Assanis, D. N., Filipi, Z. S., Fiveland, S. B., and Syrimis, M. (2003). "A predictive ignition delay correlation under steady-state and transient operation of a direct injection diesel engine." *J. Eng. Gas Turbines Power*, 125(2), 450–457.

ASTM. (1995). "Standard test method for pour point of petroleum products." *ASTM D97*, West Conshohocken, PA.
ASTM. (1999). "Standard test method for density, relative density, or API gravity of crude petroleum and liquid petroleum products by hydrometer method." *ASTM D1298*, West Conshohocken, PA.
ASTM. (2003). "Standard test methods for flash point by Pensky-Martens closed cup tester." *ASTM D93*, West Conshohocken, PA.
ASTM. (2004). "Standard test method for acid number of petroleum products by potentiometric titration." *ASTM D664*, West Conshohocken, PA.
ASTM. (2005a). "Standard test method for cetane number of diesel fuel oil." *ASTM D613*, West Conshohocken, PA.
ASTM. (2005b). "Standard test method for cloud point of petroleum products and liquid fuels." *ASTM D2500*, West Conshohocken, PA.
ASTM. (2005c). "Standard test method for water in petroleum products and bituminous materials by distillation." *ASTM D95*, West Conshohocken, PA.
ASTM. (2006). "Standard test method for kinematic viscosity of transparent and opaque liquids (and calculation of dynamic viscosity)." *ASTM D445*, West Conshohocken, PA.
ASTM. (2007). "Standard specification for biodiesel fuel blend stock (B100) for middle distillate fuels." *ASTM D6751*, West Conshohocken, PA.
ASTM. (2009). "Standard test method for determination of additive elements in lubricating oils by inductively coupled plasma atomic emission spectrometry." *ASTM D4951*, West Conshohocken, PA.
ASTM. (2013). "Standard test method for determination of total monoglycerides, total diglycerides, total triglycerides, and free and total glycerin in B-100 biodiesel methyl esters by gas chromatography." *ASTM D6584*, West Conshohocken, PA.
Barlow, T. J., Latham, S., McCrae, I. S., and Boulter, P. G. (2009). "A reference book of driving cycles for use in the measurement of road vehicle emissions." *Project Rep. PPR354*, Berkshire, U.K., ⟨https://www.gov.uk/government/uploads/system/uploads/attachment_data/file/4247/ppr-354.pdf⟩.
Chang, Y., et al. (2014). "Effects of waste cooking oil-based biodiesel on the toxic organic pollutant emissions from a diesel engine." *Appl. Energy*, 113, 631–638.
Chattopadhyay, S., and Sen, R. (2013). "Fuel properties, engine performance and environmental benefits of biodiesel produced by a green process." *Appl. Energy*, 105, 319–326.
Chen, X., Haskara, I., Wang, Y., and Zhu, G. (2014). "Detecting the combustion phase and the biodiesel blend using a knock sensor." *J. Automot. Eng.*, 222(9), 1189–1199.
Dec, J. (1997). "A conceptual model of DI diesel combustion based on laser-sheet imaging." *SAE Paper 970873*, Society of Automotive Engineers, Warrendale, PA.
Donahue, R., and Foster, D. E. (2000). "Effects of oxygen enhancement on the emissions from a DI diesel via manipulation of fuels and combustion chamber gas composition." *SAE Paper 2000-01-0512*, Society of Automotive Engineers, Warrendale, PA.
EC (European Council). 1991. "Council Directive 91/441/EEC of 26 June 1991 amending Directive 70/220/EEC on the approximation of the laws of the Member States relating to measures to be taken against air pollution by emissions from motor vehicles." *Euro 1*, Brussels, Belgium.
EC (European Council). (2007). "Regulation (EC) No 715/2007 of The European Parliament and of The Council of 20th June 2007 on type approval of motor vehicles with respect to emissions from light passenger and commercial vehicles (Euro 5 and Euro 6) and on access to vehicle repair and maintenance information." *Euro 5/Euro 6*, Strasbourg, France.
European Standard. (2003a). "Fat and oil derivatives: Fatty acid methyl esters (FAME)—Determination of iodine value." *EN 14111*, Brussels, Belgium.
European Standard. (2003b). "Fat and oil derivatives: Fatty acid methyl esters (FAME)—Determination of oxidation stability (accelerated oxidation test)." *EN 14112*, Brussels, Belgium.
European Standard. (2006). "Fat and oil derivatives: Fatty acid methyl ester (FAME)—Determination of Ca, K, Mg and Na content by optical emission spectral analysis with inductively coupled plasma (ICP OES)." *EN 14538*, Brussels, Belgium.
European Standard. (2011). "Fat and oil derivatives: Fatty acid methyl esters (FAME)—Determination of ester and linolenic acid methyl ester contents." *EN 14103*, Brussels, Belgium.
Garner, S., Sivaramakrishnan, R., and Brezinsky, K. (2009). "The high-pressure pyrolysis of saturated and unsaturated C7 hydrocarbons." *Proc. Combust. Inst.*, 32(1), 461–467.
Giakoumis, E. G., Rakopoulos, C. D., and Rakopoulos, D. C. (2014). "Assessment of NOx emissions during transient diesel engine operation with biodiesel blends." *J. Energy Eng.*, 10.1061/(ASCE)EY.1943-7897.0000136, A401400410.
Gill, S. S., Tsolakis, A., Dearn, K. D., and Rodriguez-Fernandez, J. (2011). "Combustion characteristics and emissions of Fischer-Tropsch diesel fuels in IC engines." *Prog. Energy Combust. Sci.*, 37(4), 503–523.
Guillemin, F., Grondin, O., Chauvin, J., and Nguyen, E. (2008). "Combustion parameters estimation based on knock sensor for control purpose using dedicated signal processing platform." *SAE Paper 2008-01-0790*, Society of Automotive Engineers, Warrendale, PA.
Halstead, M. P., Kirsch, L. J., Prothero, A., and Quinn, C. P. (1975). "A mathematical model for hydrocarbon autoignition at high pressures." *Proc. R. Soc. London A*, 346(1647), 515–538.
Heywood, J. (1988). *Internal combustion engine fundamentals*, McGraw-Hill, New York.
Hoekman, S. K., and Robbins, C. (2012). "Review of the effects of biodiesel on NOx emissions." *Fuel Process. Technol.*, 96(1), 237–249.
Hoskin, D., Edwards, C., and Siebers, D. (1992). "Ignition delay performance versus composition of model fuels." *SAE Paper 920109*, Society of Automotive Engineers, Warrendale, PA.
Jozsa, V., and Kun-Balog, A. (2015). "Spectroscopic analysis of crude rapeseed oil flame." *Fuel Process. Technol.*, 139, 61–66.
Kamimoto, T., and Kobayashi, H. (1991). "Combustion process in diesel engines." *Prog. Energy Combust. Sci.*, 17(2), 163–189.
Karavalakis, G., Johnson, K. C., Hajbabaei, M. H., and Durbin, T. D. (2016). "Application of low-level biodiesel blends on heavy-duty (diesel) engines: Feedstock implications on NOx and particulate emissions." *Fuel*, 181, 259–268.
Kegl, B. (2006). "Numerical analysis of injection characteristics using biodiesel fuel." *Fuel*, 85(17–18), 2377–2387.
Knothe, G., Gerpen, J. H. V., and Krahl, J. (2010). *The biodiesel handbook*, American Oil Chemists Society Press, Champaign, IL.
Knothe, G., and Razon, L. F. (2017). "Biodiesel fuels." *Prog. Energy Combust. Sci.*, 58, 36–59.
Kong, S. C., and Reitz, R. D. (1993). "Multidimensional modeling of diesel ignition and combustion using a multistep kinetics model." *J. Eng. Gas Turbines Power*, 115(4), 781–789.
Kourmatzis, A., Pham, P. X., and Masri, A. (2015). "A burner for the characterization of atomization and combustion characteristics in turbulent spray flames." *Combust. Flame*, 162(4), 978–996.
Kourmatzis, A., Pham, P. X., and Masri, A. R. (2013). "Air assisted atomization and spray density characterization of ethanol and a range of biodiesels." *Fuel*, 108, 758–770.
Kousoulidou, M., Dimaratos, A., Karvountzis-Kontakiotis, A., and Samaras, Z. (2014). "Combustion and emissions of a common-rail diesel engine fueled with HWCO." *J. Energy Eng.*, 10.1061/(ASCE)EY.1943-7897.0000154, A4013001.
Krahl, J., Baum, K., Hackbarth, U., Jeberien, H., Munack, A., and Schutt, C. (2001). "Gaseous compounds, ozone precursors, particle number and particle size distributions, and mutagenic effects due to biodiesel." *Trans ASAE*, 44(2), 179–191.
Lapuerta, M., Armas, O., and Rodriguez-Fernandez, J. (2008). "Effect of biodiesel fuels on diesel engine emissions." *Prog. Energy Combust. Sci.*, 34(2), 198–223.
Lee, D., Jho, Y., and Lee, C. S. (2014). "Effects of soybean and canola oil–based biodiesel blends on spray, combustion, and emission characteristics in a diesel engine." *J. Energy Eng.*, 10.1061/(ASCE)EY.1943-7897.0000160, A4014012.
Lee, J., Hwang, S., and Lim, J. (1998). "A new knock-detection method using cylinder pressure, block vibration and sound pressure signals from a SI engine." *SAE Technical Paper 981436*, Society of Automotive Engineers, Warrendale, PA.

Macian, V., Payri, R., Ruiz, S., Bardi, M., and Plazas, A. H. (2014). "Experimental study of the relationship between injection rate shape and diesel ignition using a novel piezo-actuated direct-acting injector." *Appl. Energy*, 118, 100–113.

Maricq, M. (2011). "Physical and chemical comparison of soot in hydrocarbon and biodiesel fuel diffusion flames: A study of model and commercial fuels." *Combust. Flame*, 158(1), 105–116.

Miyamoto, N., Ogawa, H., Nurun, N. M., Obata, I., and Arima, T. (1998). "Smokeless, low NOx, high thermal efficiency, and low noise diesel combustion with oxygenated agents as main fuel." *SAE Paper 980506*, Society of Automotive Engineers, Warrendale, PA.

Nguyen, V. H., and Pham, P. X. (2015). "Biodiesels: Oxidizing enhancers to improve C.I engine performance and emission quality." *Fuel*, 154, 293–300.

Nguyen, V. H., Vu, H. T., Do, H. M., Woo, J. Y., and Jun, H. H. (2013). "Esterification of waste fatty acid from palm oil refining process into biodiesel by heterogeneous catalysis: Fuel properties of B10, B20 blends." *Int. J. Renewable Energy Environ. Eng.*, 1(1), 1–5.

Omidvarborna, H., Kumar, A., and Kim, D.-S. (2016). "Variation of diesel soot characteristics by different types and blends of biodiesel in a laboratory combustion chamber." *Sci. Total Environ.*, 544, 450–459.

Pham, P., et al. (2013). "Engine performance characteristics for biodiesels of different degrees of saturation and carbon chain lengths." *SAE Int. J. Fuels Lubr.*, 6(1), 188–198.

Pham, P. X. (2015). "Influences of molecular profiles of biodiesels on atomization, combustion and emission characteristics." Ph.D. thesis, Aerospace, Mechanical and Mechatronic Engineering, Univ. of Sydney, Australia.

Pham, P. X., Bodisco, T. A., Ristovski, Z. D., Brown, R. J., and Masri, A. R. (2014). "The influence of fatty acid methyl ester profiles on inter-cycle variability in a heavy duty compression ignition engine." *Fuel*, 116, 140–150.

Ragland, K. W., and Bryden, K. M. (2011). *Combustion engineering*, CRC Press, Boca Raton, FL.

Rakopoulos, C. D., Kyritsis, D. C., and Rakopoulos, D. C. C. (2014). "Special issue on innovative technologies on combustion of biofuels in engines: Issues and challenges." *J. Energy Eng.*, 10.1061/(ASCE)EY.1943-7897.0000193, A2014001.

Reitz, D. (2015). "Grand challenges in engine and automotive engineering." *Front. Mech. Eng.*, 1(1), 1–3.

Rodriguez-Fernandez, J., Tsolakis, A., Ahmadinejad, M., and Sitshebo, S. (2010). "Investigation of the deactivation of a NOx-reducing hydrocarbon-selective catalytic reduction (HC-SCR) catalyst by thermogravimetric analysis: Effect of the fuel and prototype catalyst." *Energy Fuels*, 24(2), 992–1000.

Rothamer, D. A., and Murphy, L. (2013). "Systematic study of ignition delay for jet fuels and diesel fuel in a heavy-duty diesel engine." *Proc. Combust. Inst.*, 34(2), 3021–3029.

Roy, M. M., Wang, W., and Bujold, J. (2013). "Biodiesel production and comparison of emissions of a DI diesel engine fueled by biodiesel–diesel and canola oil–diesel blends at high idling operations." *Appl. Energy*, 106, 198–208.

Sabil, K. M., Aziz, M. A., Lal, B., and Uemura, Y. (2013). "Synthetic indicator on the severity of torrefaction of oil palm biomass residues through mass loss measurement." *Appl. Energy*, 111, 821–826.

Schonborn, A., Ladommatos, N., Williams, J., Allan, R., and Rogerson, J. (2009). "The influence of molecular structure of fatty acid monoalkyl esters on diesel combustion." *Combust. Flame*, 156(7), 1396–1412.

Syrimis, M., Shigahara, K., and Assanis, D. N. (2006). "Correlation between knock intensity and heat transfer under light and heavy knock conditions in a spark-ignition engine." *SAE Paper 890882*, Society of Automotive Engineers, Warrendale, PA.

Taglialatela-Scafati, F., and Lavorgna, M. (2011). "Use of vibration signal for diagnosis and control of a four-cylinder diesel engine." *Technical Paper 2011-24-0169, SAE Paper 890882*, Society of Automotive Engineers, Warrendale, PA.

Talebian-Kiakalaieh, A., Amin, N. A. S., and Mazaheri, H. (2013). "A review on novel processes of biodiesel production from waste cooking oil." *Appl. Energy*, 104, 683–710.

Tat, M. E., Gerpen, J. H. V., Soylu, S., Canakci, M., Monyem, A., and Wormley, S. (2000). "The speed of sound and isentropic bulk modulus of biodiesel at 21°C from atmospheric pressure to 35 MPa." *J. Am. Oil Chem. Soc.*, 77(3), 285–289.

Timms, R. (2007). "Palm oil—The oil for the 21st century." *Eur. J. Lipid Sci. Technol.*, 109(4), 287–288.

Tree, D. R., and Svensson, K. I. (2007). "Soot processes in compression ignition engines." *Prog. Energy Combust. Sci.*, 33(3), 272–309.

Tziourtzioumis, D. N., and Stamatelos, A. M. (2014). "Effects of B20 on the operation of a single-cylinder engine equipped with a sic diesel particulate filter." *J. Energy Eng.*, 10.1061/(ASCE)EY.1943-7897.0000144, A4014009.

Varatharajan, K., and Cheralathan, M. (2012). "Influence of fuel properties and composition on NOx emissions from biodiesel powered diesel engines: A review." *Renewable Sustainable Energy Rev.*, 16(6), 3702–3710.

Westbrook, C. K. (2013). "Biofuels combustion." *Annu. Rev. Phys. Chem.*, 64, 201–219.

Wilcox, J. (2014). "Grand challenges in advanced fossil fuel technologies." *Front. Energy Res.*, 2(47), 1–3.

Yaakob, Z., Mohammad, M., Alherbawi, M., Alam, Z., and Sopian, K. (2013). "Over view of the production of biodiesel from waste cooking oil." *Renewable Sustainable Energy Rev.*, 18, 184–193.

Yan, J., and Lin, T. (2009). "Biofuels in Asia." *Appl. Energy*, 86, S1–S10.

Zhen, D., Wang, T., Gu, F., Tesfa, B., and Ball, A. (2013). "Acoustic measurements for the combustion diagnosis of diesel engines fuelled with biodiesels." *Meas. Sci. Technol.*, 24(5), 055005.

Zhu, L., Zhang, W., Liu, W., and Huang, Z. (2010). "Experimental study on particulate and NOx emissions of a diesel engine fueled with ultra low sulfur diesel, RME-diesel blends and PME-diesel blends." *Sci. Total Environ.*, 408(5), 1050–1058.